



Research Paper

Polysulfone/Iron Oxide Nanoparticles Ultrafiltration Membrane for Adsorptive Removal of Phosphate from Aqueous Solution

Muhammad Nidzhom Zainol Abidin¹, Pei Sean Goh^{1,*}, Ahmad Fauzi Ismail¹, Noresah Said¹, Mohd Hafiz Dzarfan Othman¹, Hasrinah Hasbullah¹, Mohd Sohaimi Abdullah¹, Be Cheer Ng¹, Siti Hamimah Sheikh Abdul Kadir², Fatmawati Kamal²

¹ Advanced Membrane Technology Research Centre (AMTEC), School of Chemical and Energy Engineering, Faculty of Engineering, Universiti Teknologi Malaysia, 81310 Skudai, Johor Darul Ta'zim, Malaysia

² Institute of Medical Molecular Biotechnology (IMMB), Faculty of Medicine, Universiti Teknologi MARA Sungai Buloh Campus, Jalan Hospital, 47000 Sungai Buloh, Selangor, Malaysia

Article info

Received 2018-06-06
Revised 2018-07-25
Accepted 2018-07-30
Available online 2018-07-30

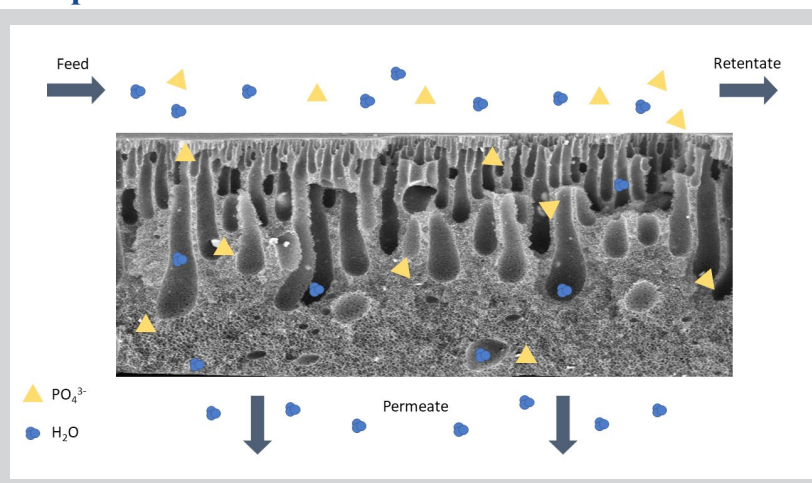
Keywords

Iron oxide nanoparticle
Ultrafiltration membrane
Phosphate removal
Wastewater treatment

Highlights

- PSf/IONPs membrane combines filtration and phosphate removal.
- Enhanced membrane water transport properties after addition of IONPs.
- IONPs interact with phosphate via electrostatic attraction.
- Maximum phosphate adsorption capacity of 73.5 mg/g membrane.
- High flux membrane with lower phosphate concentration of permeate is achieved.

Graphical abstract



Abstract

Excessive nutrient contents in water bodies renders eutrophication and causes undesired structural changes to the environment. One of the most straightforward strategies to address eutrophication issue is through the removal of nutrients such as phosphate ions from the water sources. A combination of membrane filtration and adsorption process is an attractive alternative to remove phosphate from aqueous solution. In this work, polysulfone/iron oxide nanoparticles (PSf/IONPs) adsorptive nanocomposite ultrafiltration (UF) membrane was prepared via phase separation process. Flat sheet membranes were characterized using scanning electron microscopy, energy-dispersive X-ray spectrometry, contact angle, overall pore size, porosity and pure water flux (PWF). Results showed that the incorporation of IONPs greatly enhanced the membrane PWF from 10.0 L/m²/h to 55.2 L/m²/h, contributed by the enhanced surface hydrophilicity (contact angle = 63.9°), porosity (74.1%) and larger overall pore size (79.3 nm). It was revealed that the membrane possessed phosphate adsorption capacity of 73.5 mg/g. Filtration experiment demonstrated that the PSf/IONPs membrane exhibited efficient phosphate removal under a steady flux. The design of this adsorptive UF membrane could fulfil the current necessity to remove phosphate from wastewater.

© 2019 MPRL. All rights reserved.

1. Introduction

Aquatic ecology is facing a dire concern of the high accumulation of nutrients in water which has caused eutrophication [1]. Phosphate as an essential nutrient for aquatic plants and bacteria, is one of the substances that causes this phenomenon [2]. Eutrophication is a direct cause of oxygen depletion in water that renders the deterioration of aquatic life. Due to the adverse effects of phosphate on the natural ecosystem and potential hazards on human health [3], a systematic measure to treat the excessive phosphate in

wastewater is highly needed before discharging into water streams.

Current practices to remove aqueous phosphate include chemical precipitation [4], biological treatment [5] and physical adsorption [6]. Among these methods, physical adsorption is regarded as a more efficient, practical and cost-saving approach [7]. It includes the use of materials with excellent binding affinity of phosphate. Various inorganic particles including activated carbon, metal oxides such as iron oxide and silica, metal hydroxides such as

* Corresponding author at: Phone: +60 7 553 5592; fax: +60 7 558 1463
E-mail address: peisean@petroleum.utm.my (P.S. Goh)

iron hydroxide and lanthanum hydroxide and metal oxide composites have been utilized to adsorb phosphate [6,8-10]. Iron hydroxide and manganese (II) oxide composite for example have been reported among the most efficient commercial adsorbents of phosphate, with adsorption capacity of 300 mg/g and 14.58 mg/g, respectively [8]. Despite the superior phosphate removal, a study by Gu et al. [10] discovered that the precipitation of metal and metal hydroxide into less soluble metal phosphate is greatly hindered by competitive effect of hydroxyl groups.

The major issue concerning the use of these inorganic particles alone is it requires secondary process to reclaim the suspended particles after the wastewater treatment. To counter this limitation, the immobilization of the particles within a porous membrane has been proposed to eliminate the additional process. Polymer-based membranes such as polyacrylonitrile and polyethersulfone have been employed as a host for these adsorptive particles [11,12]. Chen et al. [13] fabricated poly(vinylidene fluoride)/lanthanum hydroxide (PVDF/La(OH)₃) composite membrane for the purpose of removing phosphate. The La(OH)₃ nanorods were formed *in situ* within the membrane via phase inversion process in alkaline solution. This composite membrane recorded an adsorption capacity of 256.6 mg/g La as the La(OH)₃ turns into LaPO₄ precipitate.

Metal oxides on the other hand work differently with phosphate since they are more chemically stable as they retain their chemical state within polymers [14]. Therefore, in this study, polysulfone/iron oxide nanoparticles (PSf/IONPs) ultrafiltration (UF) membrane was fabricated via phase inversion technique for adsorptive removal of phosphate. The IONPs which acted as membrane fillers were responsible to capture the phosphate ions while the membrane performing the filtration process. This study suggested that the PSf/IONPs membrane significantly reduced the level of phosphate concentration in aqueous solution hence could potentially become a grounding solution for treatment of phosphate in wastewater.

2. Experimental

2.1. Materials

The main polymer, PSf (Udel, P1700) was procured from Solvay Advanced Polymers. Polyvinylpyrrolidone (PVP) with molecular weight of 24,000 g/mol and calcium phosphate monobasic were purchased from Sigma Aldrich. IONPs (~20 nm) were supplied by NovaScientific. N-methyl-2-pyrrolidone (NMP) was obtained from Merck.

2.2. Preparation of flat sheet membrane

PSf was first dried in an oven overnight at 50 °C. 3 wt% of PVP was dissolved in NMP by mechanical stirring at 70 °C for one hour, before 5 wt% of IONPs were added. The mixture was then vigorously stirred for 5 h to ensure a well dispersion of IONPs. Finally, 15 wt% of PSf was gradually added with a gentle stirring until the solution became homogeneous.

The prepared dope solution was cast using a glass rod on a dust-free glass plate. The nascent membrane was exposed to air for 60 s before immersing in coagulation bath (water) to complete the phase inversion process. Water was replaced daily for 3 days to remove solvent residual, before the membrane was air-dried.

2.3. Characterization of membranes

Scanning electron microscopy (SEM, Hitachi, TM3000) was utilized to observe the structural morphology of PSf/IONPs membranes. After the membranes were fractured in liquid nitrogen, sputter coating (platinum) was applied on the membrane samples prior to analysis. Energy-dispersive X-ray (EDX) spectrometer was used for elemental analysis of iron embedded in the polymer matrix. The membrane surface hydrophilicity was obtained using contact angle goniometer (OCA15pro, Dataphysics Instruments GmbH Filderstadt). The water permeation study was conducted using a cross-flow UF system. The membrane was first pressurized at 1.5 bar for at least 30 min, before the measurement was taken at 1 bar. Pure water flux (PWF) of the membrane was determined using Eq. (1).

$$J = V / (A \times \Delta t) \quad (1)$$

where J is PWF (L/m²/h), V is the permeate volume (L), Δt is permeation duration (h) and A represents the membrane effective surface area (m²). To measure the membrane porosity, dry-wet weight method was performed [15,16], and the porosity was calculated using Eq. (2).

$$\varepsilon = (w_1 - w_2) / V \rho_w \times 100\% \quad (2)$$

where ε is membrane porosity (%), w_1 and w_2 are the membrane weight at wet and dry condition, respectively. ρ_w is the water density (1.0 g/cm³) and V is the membrane volume. The overall pore size, d (m) was calculated using the modified Guerout-Elford-Ferry equation (Eq. (3)).

$$d = \sqrt{\frac{(2.9 - 1.75\varepsilon) \times 8\eta l Q}{\varepsilon \times A \times \Delta P}} \times 2 \quad (3)$$

where η is the viscosity of water at room temperature, l represents the thickness of the membrane (m), Q is the water permeation rate (m³/s), A is the membrane effective surface area (m²) and ΔP is the pressure applied (Pa).

2.4. Adsorption study

Adsorption characteristics of PSf/IONPs membrane on phosphate were investigated. Calcium phosphate solutions with concentration 0-100 mg/L were prepared in reverse osmosis (RO) water. 0.05 g of membrane was placed in a 50 mL conical flask containing 10 mL calcium phosphate solution. The mixture then was agitated at 160 rpm using an orbital shaker (Miulab, GS-20, China) at room conditions. The phosphate concentration was evaluated using photometrical detection of phosphomolybdenum blue (Nanocolor, Macherey-Nagel GmbH & Co. KG). The amount of phosphate adsorbed per unit gram of membrane was determined via Eq. (4):

$$q_e = (C_o - C_e) V / m \quad (4)$$

where q_e is the adsorbed amount of solute at equilibrium per adsorbent weight (mg/g), C_o and C_e are the initial concentration and the equilibrium concentration of solute, respectively (mg/L), m represents the initial mass of the adsorbent (g) and V represents the volume of the solution (L). The data for adsorption isotherm was fitted into non-linear regressions forms using Langmuir and Freundlich equations ((Eq. (5) and Eq. (6), respectively).

$$\frac{C_e}{q_e} = \frac{1}{Q_{max} b} + \frac{C_e}{Q_{max}} \quad (5)$$

where q_e is the adsorbed amount of phosphate at equilibrium (mg/g), C_e is the concentration of phosphate (mg/L) at equilibrium, Q_{max} denotes the maximum adsorption capacity of (mg/g) and b represents the Langmuir constant (L/g).

$$\ln q_e = \ln K_F + \left(\frac{1}{n}\right) \ln C_e \quad (6)$$

where q_e is the adsorbed amount of phosphate at equilibrium (mg/g), C_e is the concentration of phosphate (mg/L) at equilibrium, K_F denotes the Freundlich constant (mg/g) and $1/n$ represents the heterogeneity parameter. To study the kinetic of the adsorption, Lagergen's pseudo-first-order and pseudo-second-order kinetic models were employed using Eq. (7) and Eq. (8), respectively [17].

$$\log (q_e - q_t) = \log q_e - \left(\frac{k_1 t}{2.303}\right) \quad (7)$$

$$\frac{t}{q_t} = \frac{1}{k_2 q_e^2} + \frac{t}{q_e} \quad (8)$$

where q_e is the adsorbed amount of phosphate at equilibrium (mg/g) whereas q_t is the adsorbed amount of phosphate at the designated time (mg/g), t is the selected time interval (h), k_1 is the rate constant of pseudo-first-order model (1/h) whereas k_2 is the rate constant for pseudo-second-order model (g/mg.h).

2.5. UF adsorption study

The adsorption properties of the PSf/IONPs membrane in UF process were investigated by filtering 10 mg/L calcium phosphate solution using the same cross-flow UF system at the operating pressure of 1 bar. The membrane (10 cm²) was placed in the UF cell. Every 20 min, a sample of permeate was collected and its phosphate concentration was analyzed.

3. Results and discussion

3.1. Membrane characterizations

3.1.1. Morphological and elemental analyses

The structural morphology of the membranes is shown in Figure 1. Generally, a typical asymmetrical structure of PSf membrane was observed. A thin dense layer was formed at the top and supported by uniformly aligned finger-like capillaries which ended with tear drops at the middle and porous sublayer [17]. The finger-like structures of the neat PSf membrane were terminated as large cavity macroporous structures at the bottom. After blending with IONPs, a more well-defined finger-like structure can be observed with a thick layer of microporous sponge-like structure formed at the bottom. Large macrovoids in the neat membrane were hardly seen in the PSf/IONPs membrane. It could be related to the higher viscosity of PSf/IONPs dope solution [18], that restricted the formation of the large macrovoids [19]. In Figure 1-B, the presence of white clusters, claimed as IONPs can be observed at certain regions of the membrane's cross-section and surface. EDX mapping analysis (see Figure 1-C) has confirmed the identity of the clusters as IONPs, proved by the detection of Fe element. It was also noticed that the IONPs were well distributed throughout the polymer matrix.

3.1.2. Water transport properties

The contact angle, porosity, overall pore size and PWF of the membranes are tabulated in Table 1. The contact angle decreased upon the incorporation of IONPs. This justifies the hydrophilic property of IONPs owing to the presence of oxygen element in IONPs chemical structure [18]. The enhanced surface hydrophilicity of the membrane would allow better interaction with water molecules. Besides, there was an increment in the porosity of the membrane from 43.2 to 74.1%. The improved membrane porosity increased the membrane capacity to contain a larger volume of water at a time. Nanoporous structure of IONPs has certainly played its role in improving the membrane porosity by allowing water molecules to fill in the pores. This was supported by the increase of the membrane overall pore size by 66.6%. At the membrane selective skin layer, the incorporation of hydrophilic IONPs has permitted the nascent membrane to draw more air moisture during the one-min drying time. The exchange of NMP and air moistures has caused membrane precipitation with larger interconnecting pores [20]. The improvement of surface hydrophilicity, the increasing of porosity and overall pore size provided a great influence on the membrane PWF. The PSf/IONPs membrane exhibited PWF that was 5 times greater than that of neat PSf membrane, indicating the positive impact of IONPs in heightening the effectiveness of the membrane upon filtration of aqueous phosphate solution. The hydrophilic nanoporous IONPs embedded in the dense membrane skin layer have provided an alternative route for fast movement of water molecules across the membrane.

3.2. Phosphate adsorption properties

Langmuir and Freundlich adsorption curves of the PSf/IONPs membrane are shown in Figure 2-A. The data of adsorption capacity obtained from the study of the effect of various initial concentrations of phosphate can be better fitted to the Langmuir model rather than Freundlich model with correlation coefficient, R^2 value of 0.99. The phosphate ions were postulated to be deposited on the uniform, free surface of IONPs with equivalent active sites in membrane matrix. The maximum adsorption capacity, Q_{max} of the membrane, which was the reciprocal of the gradient of Langmuir linear fit, was calculated as 73.5 mg/g and the Langmuir constant, b , obtained by substituting the Q_{max} and y-intercept value of the linear fit into Eq. (5) was 0.11 L/g.

Next, the phosphate adsorption kinetics of the membrane in 100 mg/L calcium phosphate solution were measured. The adsorption capacity versus contact time plot is shown in Figure 2-B. Based on the plot, 87% of the adsorption was already achieved in the first 60 min. After 90 min, the adsorption capacity of the membrane flattened, indicating that the equilibrium phosphate concentration was reached. The R^2 (0.99) suggested that the adsorption kinetics followed the pseudo-second-order model at the rate constant of 0.084 g/mg.h. In this kinetic model, rate-limiting step is chemical reaction rather than diffusion as it depends on the concentration of both adsorbent and adsorbate [21]. The chemisorption of phosphate involved the chemical interaction between the phosphate ions and membrane surfaces. An asymmetric distribution of electrons in Fe-O and Fe=O bonds generates a partially positive Fe atom, whereas the more electronegative O atom gains the partial negative charge. Thus, the scavenging phosphate ions have most probably interacted with Fe atom via electrostatic attraction (see Figure 3), as reported by Vikrant et al. [3].

Table 2 presents the adsorption capacity of several types of adsorbent to remove phosphate. It was found that the adsorption capacity of the PSf/IONPs membrane was comparable to other developed adsorbents. Of all presented adsorbents, only 2 of them are membranes including the one prepared in this study, in which the other exhibited a very high adsorption capacity. This could be due to the excellent adsorption properties of $\text{La}(\text{OH})_3$ towards phosphate, as previously reported by He et al. [11]. However, it is worth mentioning the effectiveness of membrane towards filtration of phosphate is more important.

Table 1

Contact angle, porosity, overall pore size and PWF of the membranes.

Membrane	Contact angle (°)	Porosity (%)	Pore size (nm)	PWF (L/m ² /h)
PSf	73.5 ± 2.1	43.2 ± 2.4	47.6 ± 1.5	10.0 ± 1.8
PSf/IONPs	63.9 ± 0.8	74.1 ± 3.6	79.3 ± 2.4	55.2 ± 1.9

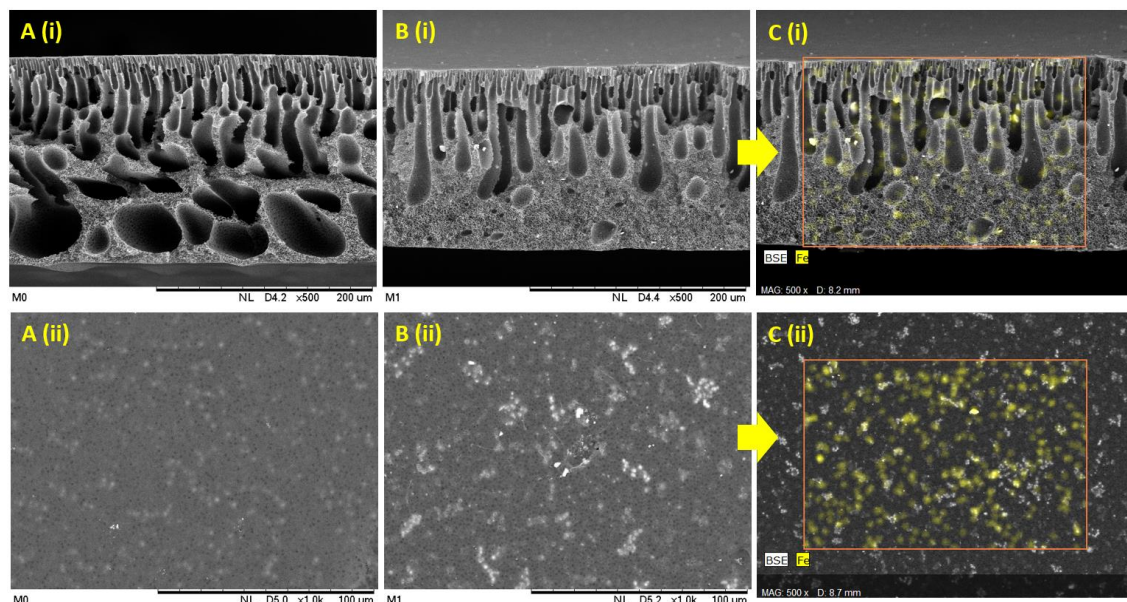


Fig. 1. Microscopic images showing (i) cross-section (ii) surface of A) PSf membrane B) PSf/IONPs membrane with C) EDX mapping of iron, Fe.

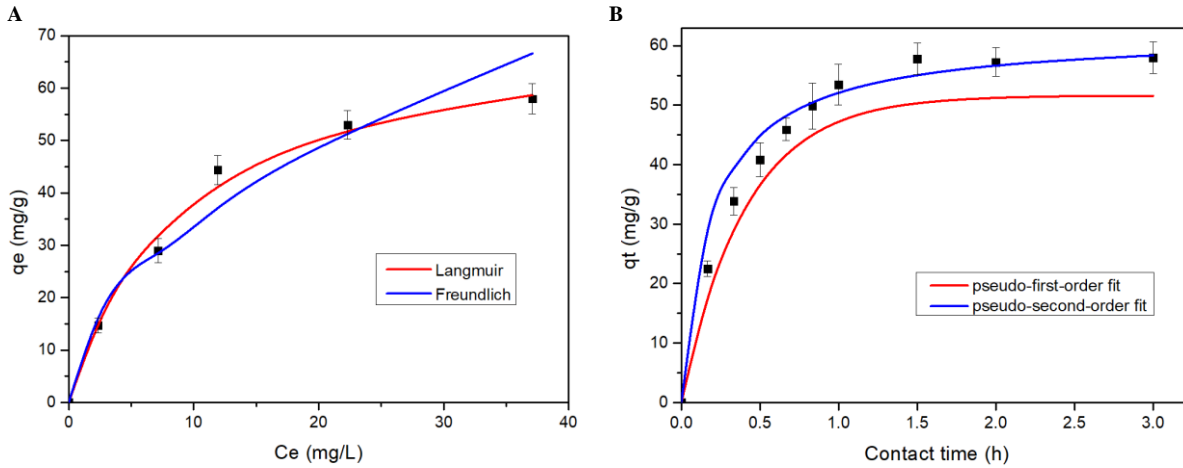


Fig. 2. (A) Phosphate adsorption isotherms of PSf/IONPs membrane ($C_0 = 20, 40, 60, 80$ and 100 mg/L). (B) Phosphate adsorption kinetics of PSf/IONPs membrane ($C_0 = 100$ mg/L).

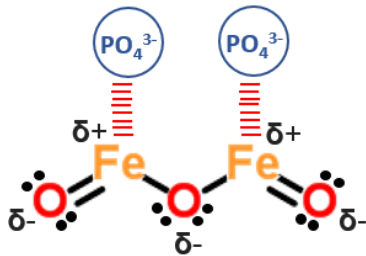


Fig. 3. Proposed interaction between IONP and phosphate ions.

Table 2
Comparison between different adsorbents for phosphate removal (pH 7, 25 °C).

Adsorbent	Dosage (g/L)	C_0 (mg/L)	q_e (mg/g)	Ref.
PSf/IONPs membrane	5.0	100	58.7	In present work
La (III)/Chitosan-montmorillonite	2.0	100	~45.0	[22]
Hydrated Fe (III)-Zr (IV) binary oxide	0.75	50	49.3	[23]
Fe-La composite	1.0	200	89.4	[24]
PVDF/La(OH) ₃ membrane	Unspecified ^a	140	256.6 ^b	[13]

^a sample size: 4 cm x 4 cm, ^b value per gram La which is 1/3 of the membrane weight.

3.3. UF separation of phosphate

The experimental results revealing both permeation and adsorption performance of PSf/IONPs membrane is shown in Figure 4-A. The first 30 min shows the values of PWF before the filtration of phosphate solution taking place. After the switching of feed solution with 10 mg/L calcium phosphate solution, the flux declined rapidly but stabilized after 130 min at ~28 L/m²/h. The quick formation of phosphate ion monolayer on the IONPs surface, as suggested by Langmuir model, has blocked the IONPs nanopores channel hence reducing the flux. In other words, the membrane was fouled by the adsorbed phosphate.

On the other hand, the blue dotted line (see Figure 4-A) displays the change of phosphate concentration in the permeate. It was noticed that the phosphate concentration in the permeate increased gradually with time in the first 30 min. Within the experiment time frame (210 min), the adsorption activity of phosphate by the membrane can be observed since the phosphate concentration detected in the permeate was lesser than in the feed, despite the reduced percent rejection of phosphate over time. This indicates that the IONPs were yet to become saturated as the adsorption performance of the membrane was governed entirely by the IONPs embedded in the membrane. After 3 h of the actual phosphate solution filtration, the membrane still rejected 37% of phosphate (see Figure 4-B), which was better than the rejection of PVDF/La(OH)₃ membrane (30%) developed by Chen et al. [13].

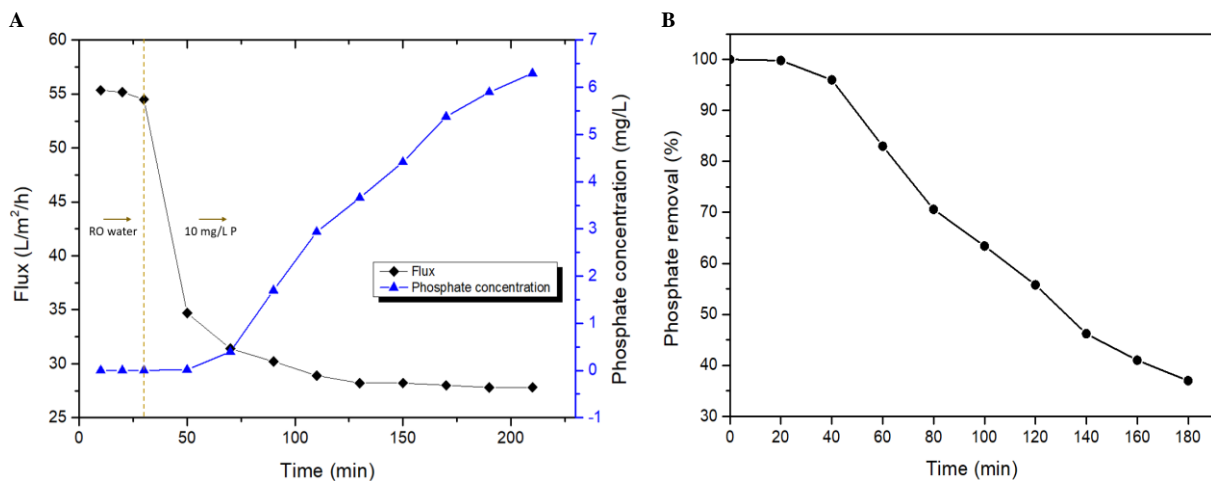


Fig. 4. (A) Membrane flux and phosphate concentration in permeate during the filtration of RO water ($t = 0-30$ min) and 10 mg/L phosphate solution ($t = 30-210$ min). (B) Phosphate removal percentage over time.

4. Conclusions

PSf/IONPs UF membrane with the capability to remove phosphate from aqueous solution has been successfully fabricated. The presence of IONPs in membrane was observed by SEM images and confirmed by EDX analysis. From SEM images, the membrane possessed a thin skin layer, finger-like structure and microporous sponge-like structure. The outstanding increment of PWF (55.2 L/m²/h) was attributed to the increased surface hydrophilicity, overall pore size and porosity of the membrane after IONPs addition. Based on the phosphate adsorption studies, the Q_{max} of the membrane was found to be 73.5 mg/g. Besides, the membrane displayed its ability to filter the phosphate solution, turning it into a higher quality water. In the future, it is hoped that the membrane could be used for a collective removal of other pollutants as well.

Acknowledgement

Authors acknowledge the financial supports provided by Ministry of Education Malaysia under HICoE Grant (Grant no: 4J183) and Universiti Teknologi Malaysia under Flagship Grant (Grant no: 01G46).

References

- [1] M. Vežjak, T. Savsek, E.A. Stuhler, System dynamics of eutrophication processes in lakes, *Eur. J. Oper. Res.* 109 (1998) 442–451.
- [2] J. Goscińska, M. Ptaszewska-Koniarz, M. Frankowski, M. Franus, R. Panek, W. Franus, Removal of phosphate from water by lanthanum-modified zeolites obtained from fly ash, *J. Colloid Interface Sci.* 513 (2018) 72–81.
- [3] K. Vikrant, K.H. Kim, Y.S. Ok, D.C.W. Tsang, Y.F. Tsang, B.S. Giri, R.S. Singh, Engineered/designer biochar for the removal of phosphate in water and wastewater, *Sci. Total Environ.* 616–617 (2018) 1242–1260.
- [4] M.R. Gaterell, R. Gay, R. Wilson, R.J. Gochin, J.N. Lester, An economic and environmental evaluation of the opportunities for substituting phosphorus recovered from wastewater treatment works in existing UK fertiliser markets, *Environ. Technol.* 21 (2000) 1067–1084.
- [5] J.H. Lv, L.J. Yuan, X. Chen, L. Liu, D.C. Luo, Phosphorus metabolism and population dynamics in a biological phosphate-removal system with simultaneous anaerobic phosphate stripping, *Chemosphere* 117 (2014) 715–721.
- [6] W. Huang, Y. Zhang, D. Li, Adsorptive removal of phosphate from water using mesoporous materials: A review, *J. Environ. Manage.* 193 (2017) 470–482.
- [7] P. Loganathan, S. Vigneswaran, J. Kandasamy, N.S. Bolan, Removal and recovery of phosphate from water using sorption, *Crit. Rev. Environ. Sci. Technol.* 44 (2014) 847–907.
- [8] L. Delgado-Velasco, V. Hernández-Montoya, N.A. Rangel-Vázquez, F.J. Cervantes, M.A. Montes-Morán, M. del R. Moreno-Virgen, Screening of commercial sorbents for the removal of phosphates from water and modeling by molecular simulation, *J. Mol. Liq.* 262 (2018) 443–450.
- [9] H. Qiu, C. Liang, J. Yu, Q. Zhang, M. Song, F. Chen, Preferable phosphate sequestration by nano-La(III) (hydr)oxides modified wheat straw with excellent properties in regeneration, *Chem. Eng. J.* 315 (2017) 345–354.
- [10] W. Gu, X. Li, M. Xing, W. Fang, D. Wu, Removal of phosphate from water by amine-functionalized copper ferrite chelated with La(III), *Sci. Total Environ.* 619–620 (2018) 42–48.
- [11] J. He, W. Wang, F. Sun, W. Shi, D. Qi, K. Wang, R. Shi, F. Cui, C. Wang, X. Chen, Highly efficient phosphate scavenger based on well-dispersed La(OH)₃ nanorods in polyacrylonitrile nanofibers for nutrient-starvation antibacteria, *ACS Nano* 9 (2015) 9292–9302.
- [12] A.C.C. Rotzetter, C.R. Kellenberger, C.M. Schumacher, C. Mora, R.N. Grass, M. Loepfe, N.A. Luechinger, W.J. Stark, Combining phosphate and bacteria removal on chemically active filter membranes allows prolonged storage of drinking water, *Adv. Mater.* 25 (2013) 6057–6063.
- [13] L. Chen, F. Liu, Y. Wu, L. Zhao, Y. Li, X. Zhang, J. Qian, In situ formation of La(OH)₃-poly(vinylidene fluoride) composite filtration membrane with superior phosphate removal properties, *Chem. Eng. J.* 347 (2018) 695–702.
- [14] L. Upadhyaya, M. Semsarilar, A. Deratani, D. Quemener, Nanocomposite membranes with magnesium, titanium, iron and silver nanoparticles - A review, *J. Membr. Sci. Res.* 3 (2017) 187–198.
- [15] M.N.Z. Abidin, P.S. Goh, A.F. Ismail, M.H.D. Othman, H. Hasbullah, N. Said, S.H.S.A. Kadir, F. Kamal, M.S. Abdullah, B.C. Ng, Antifouling polyethersulfone hemodialysis membranes incorporated with poly (citric acid) polymerized multi-walled carbon nanotubes, *Mater. Sci. Eng. C.* 68 (2016) 540–550.
- [16] M.N.Z. Abidin, P.S. Goh, A.F. Ismail, M.H.D. Othman, H. Hasbullah, N. Said, S.H.S.A. Kadir, F. Kamal, M.S. Abdullah, B.C. Ng, The effect of PCA-g-MWCNTs loading on the performance of PES/MWCNTs hemodialysis membrane, *Chem. Eng. Trans.* 56 (2017) 1609–1614.
- [17] N. Abdullah, R.J. Gohari, N. Yusof, A.F. Ismail, J. Juhana, W.J. Lau, T. Matsuura, Polysulfone/hydrous ferric oxide ultrafiltration mixed matrix membrane: Preparation, characterization and its adsorptive removal of lead (II) from aqueous solution, *Chem. Eng. J.* 289 (2015) 28–37.
- [18] N. Said, H. Hasbullah, A.F. Fauzi, M.H.D. Othman, P.S. Goh, M.N.Z. Abidin, S.H.S.A. Kadir, F. Kamal, M.S. Abdullah, B.C. Ng, Enhanced hydrophilic polysulfone hollow fiber membranes with addition of iron oxide nanoparticles, *Polym. Int.* 66 (2017) 1424–1429.
- [19] M. Homayoonfal, M.R. Mehri, M. Shariaty-Niassar, A. Akbari, A.F. Ismail, T. Matsuura, A comparison between blending and surface deposition methods for the preparation of iron oxide/polysulfone nanocomposite membranes, *Desalination* 354 (2014) 125–142.
- [20] N. Said, H. Hasbullah, A.F. Fauzi, M.N.Z. Abidin, P.S. Goh, M.H.D. Othman, S.H.S.A. Kadir, F. Kamal, M.S. Abdullah, B.C. Ng, The effect of air gap on the morphological properties of PSf/PVP90 membrane for hemodialysis application, *Chem. Eng. Trans.* 56 (2014) 1591–1596.
- [21] Y.S. Ho, G. McKay, Pseudo-second order model for sorption processes, *Process Biochem.* 34 (1999) 451–465.
- [22] H.T. Banu, P. Karthikeyan, S. Meenakshi, Lanthanum (III) encapsulated chitosan-montmorillonite composite for the adsorptive removal of phosphate ions from aqueous solution, *Int. J. Biol. Macromol.* 112 (2018) 284–293.
- [23] K. Zhou, B. Wu, L. Su, W. Xin, X. Chai, Enhanced phosphate removal using nanostructured hydrated ferric-zirconium binary oxide confined in a polymeric anion exchanger, *Chem. Eng. J.* 345 (2018) 640–647.
- [24] J. Wang, L. Wu, J. Li, D. Tang, G. Zhang, Simultaneous and efficient removal of fluoride and phosphate by Fe-La composite: Adsorption kinetics and mechanism, *J. Alloys Compd.* 753 (2018) 422–432.